

The Numerical Renormalization Group Method for correlated electrons

Ralf Bulla

Theoretische Physik III, Elektronische Korrelationen und Magnetismus, Universität Augsburg, 86135 Augsburg

Summary: The Numerical Renormalization Group method (NRG) has been developed by Wilson in the 1970's to investigate the Kondo problem. The NRG allows the non-perturbative calculation of static and dynamic properties for a variety of impurity models. In addition, this method has been recently generalized to lattice models within the Dynamical Mean Field Theory. This paper gives a brief historical overview of the development of the NRG and discusses its application to the Hubbard model; in particular the results for the Mott metal-insulator transition at low temperatures.

1 The Numerical Renormalization Group and the Kondo problem

The application of renormalization group (RG) ideas in the physics of condensed matter has been strongly influenced by the work of Wilson [1]. His 'theory for critical phenomena in connection with phase transitions' has been awarded the Nobel prize in physics in 1982 [2]. This paper deals with one aspect in the work of Wilson: the numerical renormalization group (NRG) method for the investigation of the Kondo problem.

The history of the Kondo problem [3] goes back to the 1930's when a resistance minimum was found at very low temperatures in seemingly pure metals [4]. This minimum, and the strong increase of the resistance $\rho(T)$ on further lowering the temperature, has been later found to be caused by magnetic impurities (such as iron). Kondo successfully explained the resistance minimum within a perturbative calculation for the *s-d*- (or Kondo-) model [5], a model for magnetic impurities in metals. However, Kondo's result implies a divergence of $\rho(T)$ for $T \rightarrow 0$, in contrast to the saturation found experimentally. It became clear that this shortcoming is due to the perturbative approach used by Kondo.

An important step towards a solution of this problem (the 'Kondo problem') has been the scaling approach by Anderson [6]. By successively eliminating high

energy states, Anderson showed that the coupling J in the effective low energy model diverges. However, the derivation only holds within perturbation theory in J and is therefore not necessarily valid in the large J limit. A diverging coupling between impurity and conduction electrons corresponds to a perfect screening of the impurity spin; the magnetic moment therefore vanishes for $T \rightarrow 0$ and the resistivity no longer diverges. This result has been finally verified by Wilson's NRG, as will be discussed below.

In the following, some details of the NRG method are explained in the context of the single impurity Anderson model [7] (Wilson originally set up the RG transformation for the Kondo model, but the details of the NRG are essentially the same for both models [1, 8]). The Hamiltonian of this model is given by

$$H = \sum_{\sigma} \varepsilon_f f_{\sigma}^{\dagger} f_{\sigma} + U f_{\uparrow}^{\dagger} f_{\uparrow} f_{\downarrow}^{\dagger} f_{\downarrow} + \sum_{k\sigma} \varepsilon_k c_{k\sigma}^{\dagger} c_{k\sigma} + \sum_{k\sigma} V \left(f_{\sigma}^{\dagger} c_{k\sigma} + c_{k\sigma}^{\dagger} f_{\sigma} \right). \quad (1.1)$$

In the model (1.1), $c_{k\sigma}^{(\dagger)}$ denote annihilation (creation) operators for band states with spin σ and energy ε_k , $f_{\sigma}^{(\dagger)}$ those for impurity states with spin σ and energy ε_f . The Coulomb interaction for two electrons at the impurity site is given by U and both subsystems are coupled via a hybridization V .

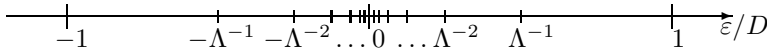


Figure 1 Logarithmic discretization of the conduction band

The first step to set up the RG-transformation is a logarithmic discretization of the conduction band (see Fig. 1): the continuous conduction band is divided into (infinitely many) intervals $[\xi_{n+1}, \xi_n]$ and $[-\xi_n, -\xi_{n+1}]$ with $\xi_n = D\Lambda^{-n}$ and $n = 0, 1, 2, \dots$. D is the half-bandwidth of the conduction band and Λ the NRG-discretization parameter (typical values used in the calculations are $\Lambda = 1.5, \dots, 2$). The conduction band states in each interval are then replaced by a *single* state. Although this approximation by a discrete set of states involves some coarse graining at higher energies, it captures arbitrarily small energies near the Fermi level.

In a second step, the discrete model is mapped on a semi-infinite chain form described by the hamiltonian (see also Fig. 2):

$$\begin{aligned}
 H &= \sum_{\sigma} \varepsilon_f f_{-1\sigma}^{\dagger} f_{-1\sigma} + U f_{-1\uparrow}^{\dagger} f_{-1\uparrow} f_{-1\downarrow}^{\dagger} f_{-1\downarrow} \\
 &+ \sum_{\sigma n=-1}^{\infty} \varepsilon_n \left(f_{n\sigma}^{\dagger} f_{n+1\sigma} + f_{n+1\sigma}^{\dagger} f_{n\sigma} \right)
 \end{aligned} \tag{1.2}$$

Here, the impurity operators are written as $f_{-1\sigma}^{(\dagger)}$ and the conduction band states as $f_{n\sigma}^{(\dagger)}$ with $n = 0, 1, 2, \dots$. Due to the logarithmic discretization, the hopping matrix elements decrease as $\varepsilon_n \propto \Lambda^{-n/2}$. This can be easily understood by considering a discretized conduction band with a finite number of states M (with M even). The lowest energy scale is, according to Fig. 1 given by $\approx D\Lambda^{-M/2}$. This discrete model is mapped onto a semi infinite chain with the same number of conduction electron degrees of freedom, M . The only way to generate the low energy scale $\approx D\Lambda^{-M/2}$ is now due to the hopping matrix elements ε_n so that they have to fall off with the square root of Lambda.

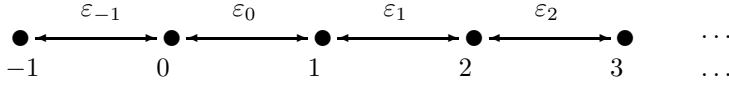


Figure 2 Semi-infinite chain form of the single impurity Anderson model

This means that, in going along the chain, the system evolves from high energies (given by D and U) to arbitrarily low energies (given by $D\Lambda^{-M/2}$). The renormalization group transformation is now set up in the following way.

We start with the solution of the isolated impurity, that is the knowledge of all eigenstates, eigenenergies and matrix elements. The first step of the renormalization group transformation is to add the first conduction electron site, set up the hamiltonian matrices for the enhanced Hilbert space, and obtain the information for the new eigenstates, eigenenergies and matrix elements by diagonalizing these matrices. This procedure is then iterated. An obvious problem occurs after only a few steps of the iteration. The Hilbert space grows as 4^N , which makes it impossible to keep all the states in the calculation. Wilson therefore devised a very simple truncation procedure in which only those states (typically a few hundred) with the lowest energies are kept. This truncation scheme is very successful but relies on the fact that the hopping matrix elements are falling off exponentially. High energy states therefore do not change the very low frequency behaviour and can be neglected.

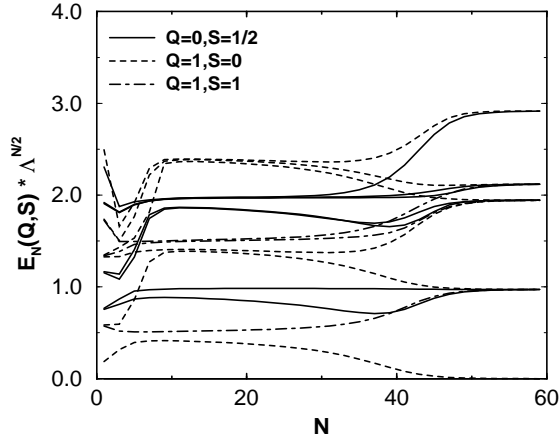


Figure 3 Flow diagram for the lowest lying energy levels for the single impurity Anderson model with $\varepsilon_f = -0.2$, $U = 0.4$ and $\Delta = 0.015$.

This procedure gives for each cluster a set of eigenenergies and matrix elements from which a number of physical properties can be derived (this will be illustrated for the calculation of the spectral function in the next section). The eigenenergies itself show the essential physics of the Kondo problem: Fig. 3 shows the dependence of the lowest lying energy levels on the length of the chain (the energies are scaled by a factor $\Lambda^{N/2}$). The system is first approaching an unstable fixed point at $N \approx 10 - 20$ (the Local Moment fixed point) and is then flowing to a stable fixed point for $N > 50$ (the Strong Coupling fixed point). By analyzing the structure of the Strong Coupling fixed point and by calculating perturbative corrections about it, Wilson (for the Kondo model [1]) and Krishnamurthy, Wilkins and Wilson (for the single impurity Anderson model [8]) found that

- i) right at the fixed point, the impurity spin is completely screened;
- ii) on approaching the fixed point, the thermodynamic properties are Fermi-liquid like; i.e. the magnetic susceptibility $\chi(T)$ approaches a constant value for $T \rightarrow 0$ and the specific heat $C = \gamma T$ is linear in T for $T \rightarrow 0$; the ratio $R = \chi/\gamma$ is known as the Wilson ratio and takes the universal value $R = 2$ in the Kondo model;

2 Developments and Applications of the NRG method

The NRG approach described so far has two main advantages: it is non-perturbative and can deal with arbitrary values of U (simply because the impurity part is diagonalized exactly); and it can describe the physics at arbitrary low energies and temperatures (due to the logarithmic discretization). This is important in Wilson's calculation for the Kondo problem which indeed showed what had been anticipated by Anderson: the development of a ground state with a completely screened impurity (the Fermi-liquid or strong-coupling fixed point). The crossover to this fixed point occurs at the Kondo scale

$$k_{\text{B}}T_{\text{K}} = D \left(\frac{\Delta}{2U} \right)^{1/2} \exp \left(-\frac{\pi U}{8\Delta} \right). \quad (2.3)$$

(This form is valid in the particle-hole symmetric case $\varepsilon_f = -U/2$; Δ is defined as $\Delta = \frac{1}{2}\pi V^2 N(E_{\text{F}})$ with $N(E_{\text{F}})$ the density of states of the conduction electrons at the Fermi level). A sufficiently large ratio U/Δ can therefore generate arbitrarily low energy scales.

On the other hand, the NRG method has one main drawback: it is only applicable to impurity type models and therefore lacks the flexibility of e.g. the Quantum-Monte-Carlo method. A typical example where the NRG fails is the one-dimensional Hubbard model. This model is very similar to the semi-infinite chain model of eq. (1.2), but with constant hopping matrix elements between neighbouring sites and a Coulomb-repulsion U on each site. One might therefore expect a similar iterative diagonalization scheme as for the hamiltonian (1.2) to work for the Hubbard model as well. However, the truncation scheme (keeping only the lowest lying states) does not work for a model where the same energy scales (U and the bandwidth) are added at each step of the RG procedure. The low energy spectrum of the cluster with one additional site now depends on states from the whole spectrum of energies of the previous iteration. (A solution to this problem, i.e. finding a truncation scheme which gives an accurate description of the larger cluster, is the Density matrix renormalization group method [9]).

There are, fortunately, a lot of interesting impurity models where the NRG can be applied and where it provided insights into a variety of physical problems. Non-Fermi liquid behaviour has been studied in the context of the Two-Channel-Kondo-Model and related models [10]. The structure of the Non-Fermi liquid fixed point as well as its stability against various perturbations has been clarified using the NRG method.

Another example is the quantum phase transition in impurity models coupling to conduction electrons with a vanishing density of states at the Fermi level: $\rho_c(\omega) \propto |\omega|^r$. Here the NRG enables a non-perturbative investigation of both the strong-coupling and local moment phases as well as the quantum critical point separating these two [11].

Apart from applying the NRG to generalized impurity models, some important technical developments have been made during the past 10 - 15 years; most notably the calculation of dynamical properties, both at zero and finite temperatures [12, 13].

Let us briefly discuss how to calculate the single-particle spectral function

$$A(\omega) = -\frac{1}{\pi} \text{Im}G(\omega + i\delta^+) , \quad \text{with} \quad G(z) = \langle\langle f_\sigma, f_\sigma^\dagger \rangle\rangle_z , \quad (2.4)$$

within the NRG approach. Due to the discreteness of the Hamiltonian, the spectral function $A(\omega)$ is given by a discrete set of δ -peaks and the general expression for finite temperature reads:

$$A_N(\omega) = \frac{1}{Z_N} \sum_{nm} \left| \langle n | f_{-1\sigma}^\dagger | m \rangle \right|^2 \delta(\omega - (E_n - E_m)) (e^{-\beta E_m} + e^{-\beta E_n}) . \quad (2.5)$$

The index N specifies the iteration number (the cluster size) and for each N the spectral function is calculated from the matrix elements $\langle n | f_{-1\sigma}^\dagger | m \rangle$ and the eigenenergies E_n, E_m . Z_N is the grand canonical partition function. Eq. (2.5) defines the spectral function for each cluster and a typical result is shown in Fig. 4.

Here, the weight of the δ -peaks in eq. (2.5) is represented by the height of the spikes. One can clearly see the typical three peak structure from the result of the 14-site cluster: charge fluctuation peaks centered at $\omega \approx \pm 0.7$ ($\omega \approx \pm U/2$) and a quasiparticle peak at the Fermi level (here $\omega = 0$). However, the resolution of the quasiparticle peak appears to be rather unsatisfactory: there is no information on the spectral density below $|\omega| \approx 0.04$. The advantage of the NRG approach (as compared to e.g. the Exact Diagonalization technique) is that by successively increasing the length of the chain, one can extract the information on the spectral density down to arbitrarily low energy scales. This is seen in the results for the $N = 16$ and $N = 18$ clusters in Fig. 4. The necessary truncation of states, as described in the previous section, is also obvious from Fig. 4. There are no excitations for $|\omega| > 0.85$ ($|\omega| > 0.45$) in the $N = 16$ ($N = 18$) cluster, so that the information on the charge fluctuation peaks is lost for the $N = 16$ and larger clusters. In order to obtain the spectral density for *all* energy scales, the data from all cluster sizes have to be put together. This means that each cluster size only provides the information on its relevant energy scale.

The resulting spectrum will still be discrete, of course, with the δ -peaks getting closer and closer together for $\omega \rightarrow 0$. It is convenient (both for using the results in further calculations and for visualizing the distribution of spectral weight) to broaden the δ -peaks in eq. (2.5) via

$$\delta(\omega - \omega_n) \rightarrow \frac{e^{-b^2/4}}{b\omega_n\sqrt{\pi}} \exp \left[-\frac{(\ln \omega - \ln \omega_n)^2}{b^2} \right] \quad (2.6)$$

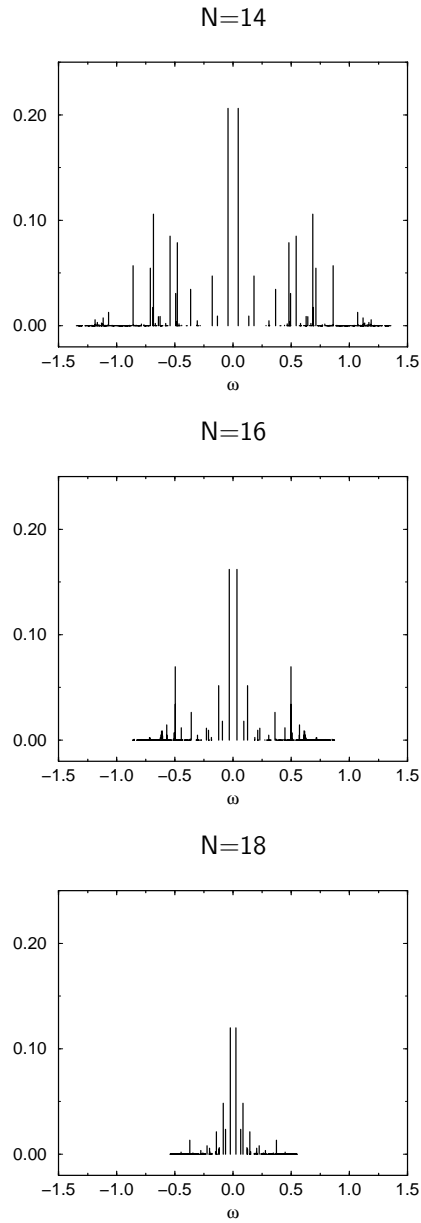


Figure 4 Spectral functions $A_N(\omega)$ for clusters with size $N = 14, 16$ and 18 . The weight of the δ -peaks is given by the height of the spikes.

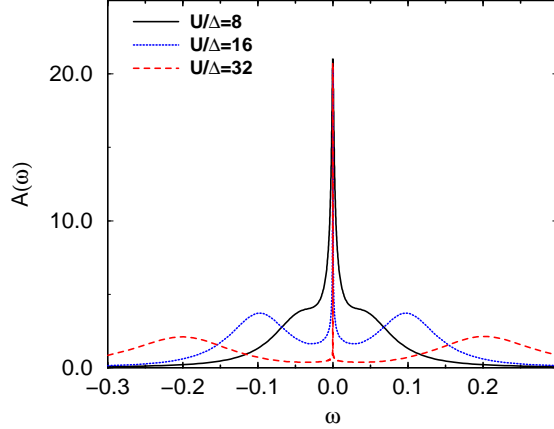


Figure 5 Spectral functions for the single impurity Anderson model for various values of U/Δ .

The broadening function is a gaussian on a logarithmic scale with width b . In this way, the broadening takes into account the logarithmic distribution of the δ -peaks.

Typical results for the spectral function of the single impurity Anderson model are shown in Fig. 5. The spectra clearly show the narrowing of the quasiparticle resonance on increasing the ratio U/Δ – corresponding to the exponential dependence of the low energy scale T_K on U/Δ .

Let us now discuss another, very important development which made it possible to apply the NRG method also to lattice models of correlated electrons: the Dynamical Mean Field Theory (DMFT).

Metzner and Vollhardt [14] showed that one can define a non-trivial limit of infinite spatial dimensions for lattice fermion models (such as the Hubbard model). In this limit, the self energy becomes purely local which allows the mapping of the lattice model onto an effective single impurity Anderson model. This impurity model has the same structure as in eq. (1.1), but the density of states of the conduction band in the impurity Anderson model has to be determined self-consistently and therefore acquires some frequency dependence. The NRG can nevertheless be applied to this case (for details see [15]). The first attempts to study the Hubbard model is the work of Sakai and Kuramoto [16]. The results obtained later by Bulla, Hewson and Pruschke [15] and Bulla [17] will be discussed in the following section.

3 NRG results for the Mott-Hubbard metal-insulator transition

The Mott-Hubbard metal-insulator transition [18, 19] is one of the most fascinating phenomena of strongly correlated electron systems. This transition from a paramagnetic metal to a paramagnetic insulator is found in various transition metal oxides, such as V_2O_3 doped with Cr [20]. The mechanism driving the Mott-Hubbard transition is believed to be the local Coulomb repulsion U between electrons on a same lattice site, although the details of the transition should also be influenced by lattice degrees of freedom. Therefore, the simplest model to investigate the correlation driven metal-insulator transition is the Hubbard model [21, 22, 23]

$$H = -t \sum_{\langle ij \rangle \sigma} (c_{i\sigma}^\dagger c_{j\sigma} + c_{j\sigma}^\dagger c_{i\sigma}) + U \sum_i c_{i\uparrow}^\dagger c_{i\uparrow} c_{i\downarrow}^\dagger c_{i\downarrow}, \quad (3.7)$$

where $c_{i\sigma}^\dagger$ ($c_{i\sigma}$) denote creation (annihilation) operators for a fermion on site i , t is the hopping matrix element and the sum $\sum_{\langle ij \rangle}$ is restricted to nearest neighbors. Despite its simple structure, the solution of this model turns out to be an extremely difficult many-body problem. The situation is particularly complicated near the metal-insulator transition where U and the bandwidth are roughly of the same order and perturbative schemes (in U or t) are not applicable.

The DMFT has already been briefly described in section 2; this method enabled a very detailed analysis of the phase diagram of the infinite-dimensional Hubbard model [24, 25]. The nature of the Mott-transition, however, has been the subject of a lively debate over the past five years (see [26, 27, 28, 29, 30]). This debate focusses on the existence (or non-existence) of a hysteresis region at very low temperatures. In such a region, two stable solutions of the DMFT equations should exist: a metallic and an insulating one. This scenario has been proposed by Georges et al. based on calculations using the Iterated Perturbation Theory (IPT), Quantum Monte Carlo and Exact Diagonalization [24]. The validity of this result has been questioned by various authors [27, 28, 29].

Let us now discuss the NRG results for the infinite dimensional Hubbard model, first of all for $T = 0$. The spectral function $A(\omega)$ for the Bethe lattice is shown in Fig. 6 for $U = 0.8U_c$, $U = 0.99U_c$ and $U = 1.1U_c$ ($U_c \approx 1.47W$, W : bandwidth) In the metallic phase (for large enough values of U) the spectral function shows the typical three-peak structure with upper and lower Hubbard bands centered at $\pm U/2$ and a quasiparticle peak at the Fermi level. For $U = 0.99U_c$, the quasiparticle peak in both Bethe and hypercubic lattice seems to be isolated (within the numerical accuracy) from the upper and lower Hubbard bands, similar to what has been observed in the IPT calculations for the Bethe lattice [24]. Consequently, the gap appears to open discontinuously at the critical U (whether the

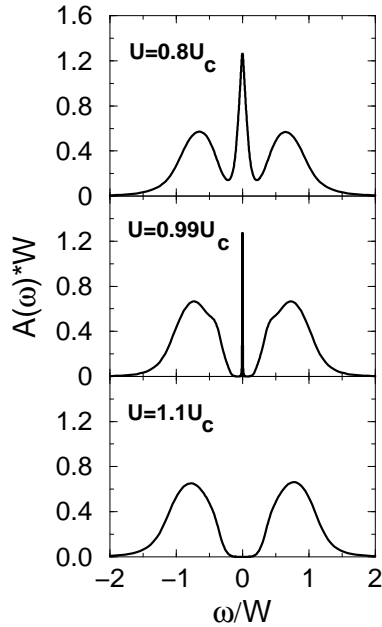


Figure 6 Spectral functions for Bethe lattice for various values of U . A narrow quasiparticle peak develops at the Fermi level which vanishes at the critical $U_c \approx 1.47W$.

spectral weight between the Hubbard bands and the quasiparticle peak is exactly zero or very small but finite cannot be decided with the numerical approach used here).

The quasiparticle peak vanishes at $U_c \approx 1.47W$ in excellent agreement with the results from the Projective Self-consistent Method (PSCM) [24, 31] $U_c \approx 1.46W$. Coexistence of metallic and insulating solutions in an interval $U_{c,1} < U < U_{c,2}$ is also found within the NRG approach. Starting from $U = 0$, the metal to insulator transition occurs at the critical $U_{c,2}$ with the vanishing of the quasiparticle peak. Starting from the insulating side, the insulator to metal transition happens at $U_{c,1} < U_{c,2}$ (the NRG and IPT give $U_{c,1} \approx 1.25W$ for the Bethe lattice).

The NRG method for the Hubbard model has only recently been generalized at finite temperatures [32]. Preliminary results for the spectral function are shown in Fig. 7 for $T = 0.00625W$ and *increasing* values of U . The upper critical U is given by $U_{c,2} \approx 1.24W$ and the transition at $U_{c,2}$ is of first order, i.e. associated with a transfer of spectral weight. The ‘insulator’ for $U > U_{c,2}$ does not develop

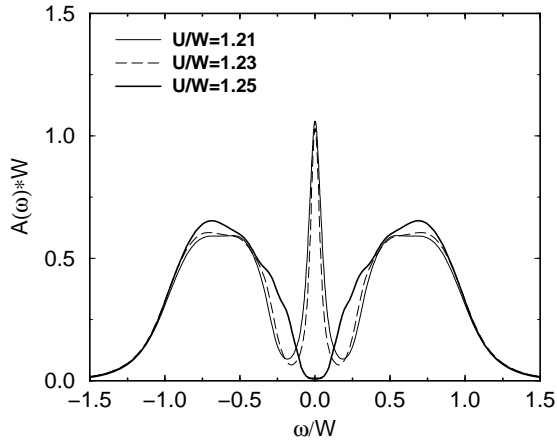


Figure 7 Spectral functions for $T = 0.00625W$ and *increasing* values of U .

a full gap (this is only possible for $U \rightarrow \infty$ or $T \rightarrow 0$), but the corresponding transport properties in this temperature range will be certainly insulating-like.

For this temperature, the NRG again finds two stable solutions in an interval $U_{c,1}(T) < U < U_{c,2}(T)$: a metallic one, with a quasiparticle peak at the Fermi level and an ‘insulating’ one, with very small spectral weight at the Fermi level (not shown here). The exact shape of the hysteresis region has still to be determined and will be discussed elsewhere [32].

What we have seen in this section is that the NRG-method (together with the DMFT) can be applied to the infinite-dimensional Hubbard model and allows a non-perturbative calculation of dynamical properties. The calculations can be performed for arbitrary interaction strength and temperature, so that the phase diagram can be (in principle) determined in the full parameter space.

4 Further developments of the NRG method

As we have discussed in the previous sections, Wilson’s NRG can be applied to two different classes of problems: impurity models and lattice models (the latter ones, however, only within the DMFT).

Concerning impurity models, the NRG has provided important theoretical insight for a variety of problems and certainly will do so in the future. In the light of the increasing possibilities of experimental fabrication, new classes of impurity models are becoming of interest. The behaviour of electrons in quantum dots,

for example, can be interpreted as that of an impurity in a conduction band (for an application of the NRG method to this problem, see [33]). Magnetic impurities can also serve as sensors, put into certain materials in a controlled way. Here one might think of impurities in a correlated host [34], or impurities in a superconducting or magnetic medium. A lot of theoretical work in applying the NRG method to these problems still needs to be done.

The second class of models are lattice models within the DMFT. Here, the NRG allows (at least in principle) the calculation of a large set of experimentally relevant quantities for a wide range of parameters (especially low temperatures and strong correlation) for a large class of models. Apart from the application to the Hubbard model which has been briefly discussed in section 3, the NRG has already been applied to the periodic Anderson model [35] and to the problem of charge ordering in the extended Hubbard model [36]. Future work will focus on generalizing the NRG method to magnetically ordered states and to systems with a coupling to (dynamical) phonons.

Of particular interest is the generalization of the NRG to multi-band models. In this way, the NRG could further extend the range of applicability of the LDA+DMFT approach [37]. Here, the non-interacting electronic band structure as calculated by the local density approximation is taken as a starting point, with the missing correlations introduced via the DMFT. On a more fundamental level, the basic physics of multi-band models at low temperatures still needs to be clarified, and again, the NRG is the obvious choice for investigating such models in the low T and intermediate to large U regime.

The author would like to thank T. Costi, D.E. Logan, A.C. Hewson, W. Hofstetter, M. Potthoff, Th. Pruschke, and D. Vollhardt for stimulating discussions and collaboration over the past few years. Part of this work was supported by the Deutsche Forschungsgemeinschaft, grant No. Bu965-1/1 and by the Sonderforschungsbereich 484.

Bibliography

- [1] K.G. Wilson, *Rev. Mod. Phys.* **47**, 773 (1975).
- [2] K.G. Wilson, in *Nobel lectures in physics 1981 - 1990* (World Scientific, Singapore 1993).
- [3] A.C. Hewson, *The Kondo Problem to Heavy Fermions* (Cambridge Univ. Press, Cambridge 1993).
- [4] W.J. de Haas, J.H. de Boer, and G.J. van den Berg, *Physica* **1**, 1115 (1934).
- [5] J. Kondo, *Prog. Theor. Phys.* **32**, 37 (1964).
- [6] P.W. Anderson, *J. Phys. C* **3**, 2439 (1970).
- [7] P.W. Anderson, *Phys. Rev.* **124**, 41 (1961).

- [8] H.R. Krishna-murthy, J.W. Wilkins, and K.G. Wilson, Phys. Rev. B **21**, 1003 (1980); **21**, 1044 (1980).
- [9] *Density-Matrix Renormalization*, eds. I. Peschel et al. (Springer, Berlin 1999).
- [10] D.M. Cragg, P. Lloyd, and Ph. Nozières, J. Phys. C **13**, 803 (1980); H.-B. Pang, D.L. Cox, Phys. Rev. B **44**, 9454 (1991). R. Bulla, A.C. Hewson, and G.-M. Zhang, Phys. Rev. B **56**, 11721 (1997).
- [11] K. Chen, C. Jayaprakash, J. Phys.: Condens. Matter **7**, L491 (1995); K. Ingersent, Phys. Rev. B **54**, 11936 (1996); R. Bulla, Th. Pruschke, and A.C. Hewson, J. Phys.: Condens. Matter **9**, 10463 (1997). R. Bulla, M.T. Glossop, D.E. Logan, and Th. Pruschke, preprint cond-mat/9909101 (1999).
- [12] O. Sakai, Y. Shimizu, and T. Kasuya, J. Phys. Soc. Jpn. **58**, 3666 (1989).
- [13] T.A. Costi, A.C. Hewson, and V. Zlatic, J. Phys.: Cond. Matter **6**, 2519 (1994).
- [14] W. Metzner and D. Vollhardt, Phys. Rev. Lett. **62**, 324 (1989); for an introduction, see D. Vollhardt, Int. J. Mod. Phys. B **3**, 2189 (1989).
- [15] R. Bulla, A.C. Hewson, and Th. Pruschke, J. Phys.: Cond. Matter **10**, 8365 (1998).
- [16] O. Sakai and Y. Kuramoto, Sol. Stat. Comm. **89**, 307 (1994).
- [17] R. Bulla, Phys. Rev. Lett. **83**, 136 (1999).
- [18] N.F. Mott, Proc. Phys. Soc. London A **62**, 416 (1949); *Metal-Insulator Transitions*, 2nd ed. (Taylor and Francis, London 1990).
- [19] F. Gebhard, *The Mott Metal-Insulator Transition*, Springer Tracts in Modern Physics Vol. 137 (Springer, Berlin 1997).
- [20] D.B. McWhan and J.P. Remeika, Phys. Rev. B **2**, 3734 (1970); D.B. McWhan, A. Menth, J.P. Remeika, Q.F. Brinkman and T. M. Rice, Phys. Rev. B **7**, 1920 (1973).
- [21] J. Hubbard, Proc. R. Soc. London A **276**, 238 (1963).
- [22] M.C. Gutzwiller, Phys. Rev. Lett. **10**, 59 (1963).
- [23] J. Kanamori, Prog. Theor. Phys. **30**, 275 (1963).
- [24] A. Georges, G. Kotliar, W. Krauth, and M.J. Rozenberg, Rev. Mod. Phys. **68**, 13 (1996).
- [25] M. Jarrell, Phys. Rev. Lett. **69**, 168 (1992); T. Pruschke, M. Jarrell, and J.K. Freericks, Adv. Phys. **44**, 187 (1995).
- [26] D.E. Logan and Ph. Nozières, Phil. Trans. R. Soc. London A **356**, 249 (1998).
- [27] S. Kehrein, Phys. Rev. Lett. **81**, 3912 (1998).
- [28] R. Noack and F. Gebhard, Phys. Rev. Lett. **82**, 1915 (1999).
- [29] J. Schlipf, M. Jarrell, P.G.J. van Dongen, S. Kehrein, N. Blümer, Th. Pruschke, and D. Vollhardt, Phys. Rev. Lett. **82**, 4890 (1999).
- [30] M.J. Rozenberg, R. Chitra, and G. Kotliar, Phys. Rev. Lett. **83**, 3498 (1999).
- [31] G. Moeller, Q. Si, G. Kotliar, M. Rozenberg, and D. S. Fisher, Phys. Rev. Lett. **74**, 2082 (1995).
- [32] R. Bulla, T.A. Costi, and D. Vollhardt, in preparation.

-
- [33] J. von Delft, U. Gerland, T.A. Costi, and Y. Oreg, preprint cond-mat/9909401 (1999).
 - [34] W. Hofstetter, R. Bulla, and D. Vollhardt, preprint cond-mat/9912396 (1999).
 - [35] Th. Pruschke, R. Bulla, and M. Jarrell, preprint cond-mat/0001357.
 - [36] R. Pietig, R. Bulla, and S. Blawid, Phys. Rev. Lett. **82**, 4046 (1999).
 - [37] V.I. Anisimov, A.I. Poteryaev, M.A. Korotin, A.O. Anokhin, and G. Kotliar, J. Phys.: Condens. Matter **9**, 7359 (1997); A.I. Lichtenstein and M.I. Katsnelson, Phys. Rev. B **57**, 6884 (1998); M.B. Zöfl, Th. Pruschke, J. Keller, A.I. Poteryaev, I.A. Nekrasov, and V.I. Anisimov, preprint cond-mat/9909359; M.I. Katsnelson and A.I. Lichtenstein preprint cond-mat/9904428; I.A. Nekrasov, K. Held, N. Blümer, V.I. Anisimov, and D. Vollhardt, in preparation.